IEEE Access
Multidisciplinary ⋮ Rapid Review ⋮ Open Access Journal

Received May 2, 2022, accepted May 27, 2022, date of publication June 3, 2022, date of current version June 16, 2022.

Digital Object Identifier 10.1109/ACCESS.2022.3179984

Control of Multiple-UAV Conveying Slung Load With Obstacle Avoidance

ABDULRAHMAN ALIYU AND SAMI EL FERIK

Department of Control and Instrumentation Engineering, King Fahd University of Petroleum and Minerals (KFUPM), Dhahran 31261, Saudi Arabia
Interdisciplinary Research Center for Smart Mobility and Logistics, KFUPM, Dhahran 31261, Saudi Arabia

Corresponding author: Sami El Ferik (selferik@kfupm.edu.sa)

This work was supported by the King Fahd University of Petroleum and Minerals, and Interdisciplinary Research Center for Smart Mobility and Logistics (KFUPM) under Project INML2200.

ABSTRACT Quadrotor Unmanned Aerial Vehicles (UAVs) are generally underactuated systems and when load is attached for transportation purposes, the system complexity increases. Therefore, the need to appropriately control such systems becomes paramount as they usually navigate in cluttered environments. In this work, we conceptualize the problem of cooperative tracking control for a Multi-agent UAV load system (MUAVLs) whereby each UAV is divided into global position and local attitude subsystems. To ensure that formation is maintained in a desired path, Neural Network Graph-theoretic Distributed Adaptive Control (NNGDAC) is used for the position subsystem with a modified virtual force artificial potential field for obstacle avoidance. Another Adaptive Feedback Linearization (AFBL) controller is also designed for the attitude subsystem which is verified by simulation results.

INDEX TERMS UAVs, multi-agent systems, intelligent control, graph theory, load transportation.

I. INTRODUCTION

Over the past few years, unmanned aerial vehicles (UAVs) have been employed in numerous fields for various applications springing from both civilian and military purposes. Examples of such applications are delivery, surveillance, fumigation, traffic monitoring, construction purposes for example pick and place objects, rescue missions, patrolling forests in case of fire outbreak, warfare, and other risky missions [1]. However, the more adapted they are to an environment the more versatile they become. The major advantages of UAVs is that it does not require a particular airfield base and they are free from rugged terrains experienced by ground robots.

A UAV is generally an underactuated system having four inputs but with six degrees of freedom comprising of position and attitude orientation. However, the degrees of freedom increases when two or more UAVs are combined to carry a load as a multi-agent system. Multi-agent UAV-load (MUAVLs) systems are those with more than one UAV concurrently conveying an attached or suspended load. These systems are highly non-linear in nature and are difficult to characterize due to the complexity their aerodynamics [2]. However, they poses some advantages over single UAV-load system due to their redundancy and ability to carry heavier payloads. Such a system requires a controller for each UAV, a formation strategy and collision avoidance which is paramount for execution of clinical tasks. This is indeed a difficult task given the nature of the system. However, several efforts have been made to address the problems associated with controlling such a system. For example, some linear control techniques such as Proportional, Integral and Differential (PID) [3]–[5] have been used to tackle the control complexity. In [3], a null space-based approach was utilized for the formation of two UAVs, whereby a multi-objective task such as collision avoidance, wind perturbation and load weight distribution were catered for with the help of PID/Adaptive and Kinematic formation controller. In [4] similar authors presented an extension with four UAVs. Cooperative transport based on PID control for the system of a four UAV arrangement, whereby the cable force computation is formulated as an optimization problem which was demonstrated in [5]. However, PID controllers are not robust to inherent disturbances that is caused by the load.

Linear Quadratic Regulator (LQR) [6], [7] and Model Predictive Control (MPC) [8] have been used with different MUAVLs system structure for transportation purposes. These methods involves linearization of the system which has some limitations. However, such control methods have been applied. For a MUAVLs system with two UAVs based

The associate editor coordinating the review of this manuscript and approving it for publication was Min Wang.

on Lagrangian model, a combination of LQR/Feedback Linearization (FBL) controllers were used in [9], whereby visual and inertial cues are used as sensing methods to avoid explicit communication between the collaborating robots. Based on Udwadia–Kalaba modeling method, a LQR-PID was designed for a formulation of MUAVLs involving four UAVs by the authors in [10], whereby swing suppression was considered and formation is maintained while guiding the load through a desired path.

The nonlinear control strategy applied are extensively FBL for multiple UAVs with suspended load [11]–[14]. In [11], a system of 4 UAVs connected to a single load whereby the load's movable center of mass was considered in a leader follower formation scheme. A coordinate free formation based on was employed in [12] in which a fictitious repulsion force for collision avoidance was introduced between two UAVs cooperatively transporting a load with the aid of a PID and geometric controller. However, repulsive forces could potentially cause oscillation in movement between connected agents. In [13], an MPC based control for a decentralized dual UAV-load system utilizing a magnetic gripper to perform search, pick up, and relocate objects with minimum communication was adopted by means of blob detection, inverse 3D-projection, Kalman filtering and visual-servoing. For a two UAV system, FBL was used for trajectory tracking, load swing suppression and obstacle avoidance whereby potential field is used to maintain inter-agent distance [14]. However, FBL may not be robust against disturbances [15] which are in fact inevitable.

A passivity based formation control strategy with internal feedback control was employed in [16] for three MUAVL. Similar control technique was utilized by the same authors [17], but environmental wind disturbance was considered. In an experimental setup [18], coordinated three MUAVLs independently to detect, track, and pick-up moving and static objects using monocular camera images and an EPM gripper whereby a reactive collision avoidance between agents was implemented. In [19], a cooperative control law is developed to control the motion of two MUAVLs and load swing with the using two PID controllers. In a slung-load dynamics obtained by Newtonian approach with spherical coordinates the authors in [20] implemented parameter-robust Linear quadratic Gaussian / Loop Transfer Recovery (LQG/LTR) to control the position and attitude of all the vehicles and payloads of a dual MUAVLs to showcase the controller's robustness against variation of payload mass.

Using three MUAVLs in [21], wrench analysis techniques used in traditional cable-driven parallel robots to account for the constraints of quadrotor actuation and dynamics in a bid to demonstrate and evaluate the design and operating configurations. A geometric feedback controller based on relative and inertial formation for 6 UAVs was adopted to track the yaw angle, cable orientation and a reference trajectory for the load's position and orientation in [22], however, geometric control has only been applied to cases where the number of are greater than two. In order to avoid singularities and complexities associated with local parameters, a coordinate free dynamical model was used. Another cascade control with decoupled attitude from the rest of the system was used in [23] but obstacle avoidance was not considered.

Load disturbance affects the UAVs which is already input handicapped, and concurrently containing load swing increases its complication. According to [24], it is mandatory to use some form of hierarchical control to handle the disturbances generated by the interaction of the vehicles and the load while they are moving. Thus, the main contribution of this includes;

1) Building a relationship between the position error of the MUAVLs based on the NNGDAC to generate inter-agent collision free trajectory.
2) Decoupling the MUAVLs into two subsystems, translational and rotational and designing a NNGDAC which is robust to load disturbance while maintaining inter-agent distance for the translational subsystem. An AFBL is also utilized to control the rotational subsystem.
3) Obstacle avoidance using a modified artificial potential field with a virtual force.

In summary, the following objectives are to be achieved;

1) Maintain inter-agent collision free formation pattern.
2) Track the desired trajectory.
3) Load disturbance rejection/Load swing suppression.
4) Obstacle avoidance.

Our approach ensures oscillation free movement between the two UAVs carrying load unlike the methods in [3] in which undesirable oscillation between agents is glaring which can lead to collision, destruction and hence termination of a mission. In [14], a simplified model of a UAV was utilized in a MUAVLs but potential field method was used to maintain inter-agent collision avoidance. However, this may lead to oscillation due to the conflict that results between attractive/repulsive forces. To ensure formation behaviors are robust against undesired side effect of the repulsive forces, H_∞ analysis was implemented by considering repulsive forces as the disturbance inputs [25] but oscillation between agents was still glaring in addition to the fact that a linearized system was utilized. However, UAVs were not utilized neither did the authors consider load swings. Conventional flocking algorithms [26] induces oscillation as evident in the results presented in [27], however load disturbances or obstacle avoidance were not considered also.

This work is summarized as follows; section I presents an introduction highlighting the literature for control of MUAVLs. Modeling of the UAV-load system is given in section II. In section III, the preliminaries to control design is presented followed by NNGDAC design for the translational subsystem together with an AFBL for the attitude subsystem in IV. Obstacle avoidance technique based on a modified artificial potential field is given in V, while the simulation results and concluding remarks are then presented in sections VI and VII respectively.

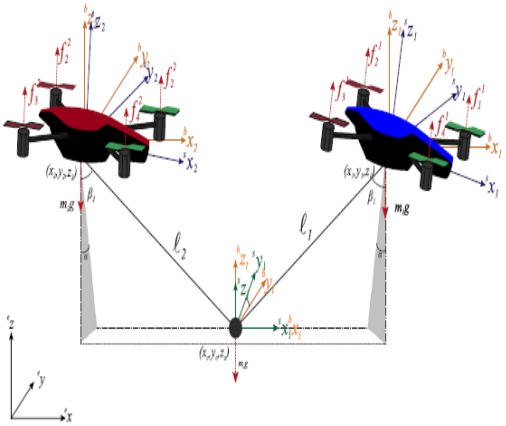

FIGURE 1. Dual UAV with Load [14].

II. MODELING

Essentially all methods for obtaining equations of motion are equivalent. However, the ease of use of the various methods differs as some are more flexible and better suited for multibody dynamics than others. Quadrotor modeling has been presented in a number of works [28] but for the purpose of completeness we present a detailed modeling of the Newton-Euler formulation in the next subsection under the following assumptions;

1) The cable is rigid and mass-less.
2) The load has no effect on the UAV while it is on the ground.
3) The load yaw angle is defined by the line connecting the two UAVs.
4) Negligible aerodynamic effects on the load and UAVs.

A. QUADROTOR AND LOAD MODEL

Consider the diagram Fig. 1. Consider that the center of mass of the quadrotor aligns with the inertial and body fixed frame which is taken as the origin.

The position in the inertial frame is represented by $\zeta = [x, y, z]$ rotational Euler angles (roll, pitch and yaw) are represented $\xi = [\phi, \theta, \psi]$. The rotation matrix R gives the transformation from body fixed frame to the inertial frame.

$$R = \begin{pmatrix} c_\psi c_\theta & c_\psi s_\theta s_\phi - s_\psi c_\phi & c_\psi s_\theta c_\phi + s_\psi s_\theta \\ s_\psi c_\theta & s_\psi s_\theta s_\phi - c_\psi c_\phi & s_\psi s_\theta c_\phi - c_\psi s_\theta \\ -s_\theta & c_\theta s_\phi & c_\theta c_\phi \end{pmatrix}$$

The thrust force generated by each rotor, $i(i = 1, 2, 3, 4)$ $T = b.f_i^2$, where d and f_i are the thrust factor and rotor speed respectively. Therefore differential equation for the acceleration of the quadrotor translational axis is thus given by;

$$\ddot{\zeta} = -g \begin{pmatrix} 0 \\ 0 \\ 1 \end{pmatrix} + R(1/m_q)T \begin{pmatrix} 0 \\ 0 \\ 1 \end{pmatrix} \tag{1}$$

where $T = d\sum_{i=1}^{4} f_i^2$ is the total thrust produced by the quadrotor, g is acceleration due to gravity and m_q is the mass of the quadrotor. Consider an inertia matrix is given by $I = diag[I_x, I_y, I_z]$, with I_x, I_y, I_z, representing the moment of inertia of the UAV. M_T is a vector describing the torque applied to the quadrotor body and M_G representing the gyroscopic torques the rotational set of differential equation is obtained as:

$$I\ddot{\xi} = -(\dot{\xi} \times I\dot{\xi}) - M_G - M_T \tag{2}$$

M_T is given by;

$$M_T = \begin{pmatrix} Lb(f_2^2 - f_4^2) \\ Lb(f_1^2 - f_3^2) \\ d(f_1^2 + f_3^2 - f_2^2 - f_4^2) \end{pmatrix}$$

with the drag factor d and the length L of the lever and M_G is given by;

$$M_G = I_R(\dot{\xi} \times \begin{pmatrix} 0 \\ 0 \\ 1 \end{pmatrix})(f_1 - f_2 + f_3 - f_4) \tag{3}$$

The overall dynamic equation therefore yields [28];

$$\begin{aligned} \ddot{x} &= \frac{1}{m_q}(\cos\phi \sin\theta \cos\psi + \sin\phi \sin\psi)u_1 + ds_1 \\ \ddot{y} &= \frac{1}{m_q}(\cos\phi \sin\theta \sin\psi + \sin\phi \cos\psi)u_1 + ds_2 \\ \ddot{z} &= -g + \frac{1}{m_q}(\cos\phi \cos\theta)u_1 + ds_3 \\ \ddot{\phi} &= \dot{\phi}\dot{\theta}\frac{(I_y - I_z)}{I_x} - \frac{J_R}{I_x}\dot{\theta}g(u) + \frac{L}{I_x}u_2 \\ \ddot{\theta} &= \dot{\phi}\dot{\psi}\frac{(I_z - I_x)}{I_y} + \frac{J_R}{I_y}\dot{\phi}g(u) + \frac{L}{I_y}u_3 \\ \ddot{\psi} &= \dot{\phi}\dot{\theta}\frac{(I_x - I_y)}{I_z} + \frac{1}{I_z}u_4 \end{aligned} \tag{4}$$

J_R represents the rotor inertia. The transformed inputs $\boldsymbol{u} = (u_1, u_2, u_3, u_4)^T$ is given by;

$$\boldsymbol{u} = \begin{pmatrix} b(f_1^2 + f_2^2 + f_3^2 + f_4^2) \\ b(f_2^2 - f_4^2) \\ b(f_1^2 - f_3^2) \\ d(f_1^2 + f_3^2 - f_2^2 - f_4^2) \end{pmatrix}$$

with $g(\boldsymbol{u}) = (f_1 - f_3 + f_2 - f_4)$. Each quadrotor $(i = 1, 2)$ is divided into two subsystems, the outer and inner loop, $\ddot{\zeta}_i$ and $\ddot{\xi}_i$ comprising the translation and rotational axis respectively. Therefore, equation (4) can be written as

$$\begin{aligned} \ddot{\zeta} &= f(\xi, u) + Ds, \text{ and} \\ \ddot{\xi} &= f(\xi) + g(u) \end{aligned} \tag{5}$$

where $Ds = [ds_1, ds_2, ds_3]'$, represent external load disturbances. From equation (4), the desired angles can be derived as [29];

$$\begin{aligned} \theta_d &= arctan(\frac{u_x cos\psi_d + u_y sin\psi_d}{u_z + g}) \\ \phi_d &= arcsin(\frac{u_x sin\psi_d - u_y cos\psi_d}{\sqrt{(u_x^2 + u_y^2) + (u_z + g)^2}}) \end{aligned} \tag{6}$$

FIGURE 2. Graph of both agents.

where u_x, u_y, u_z are the virtual control input to be discussed in subsequent section. The cable suspended load carried is modeled as [14];

$$m_l I \ddot{\zeta}_l + G_l = R_l S_l \tag{7}$$

where m_l is the load mass, $S_l = [S_1 \quad S_2]^T$ and

$$R_L = \begin{pmatrix} sin\beta_1 cos\alpha & sin\beta_2 cos\alpha \\ sin\beta_1 sin\alpha & sin\beta_2 sin\alpha \\ cos\beta_1 & cos\beta_2 \end{pmatrix}$$

Thus the disturbances on each UAV becomes;

$$Ds_i = \begin{pmatrix} S_i sin\beta_i cos\alpha \\ S_i sin\beta_i sin\alpha \\ S_i cos\beta_i + m_l g \end{pmatrix} \tag{8}$$

where α is the load lateral oscillation angle and β_i which are formed by the normal axis centered in the load center and the cables, for $S_i (i = 1, 2)$ is the cable tension given by [12];

$$S_1 = m_c g \frac{\sin \beta_2}{\sin \beta_1 + \beta_2}$$
$$S_2 = m_c g \frac{\sin \beta_1}{\sin \beta_1 + \beta_2}$$

It is important to state that the tension affects the quadrotors only when the it lifts beyond the length of the cable.

III. PRELIMINARIES

A. GRAPH THEORY

Consider a simple directed graph $G = (V, E)$ with a nonempty finite set of vertices or nodes (whereby each quadrotor translational subsystem for each is a vertice ζ_{ij}) $V = \zeta_{ij}$ and a finite set of edges $E \subseteq V \times V$. The laplacian matrix is given by $L = D - A$, where the diagonal in-degree matrix D is given by $D = diag\{d_i\}$ with $d_i = \sum_j a_{ij}$ and the adjacency matrix A, as $A = [a_{ij}]$ with $a_{ij} = 1$ if $(v_i, v_j) \in E$ and $a_{ij} = 0$ otherwise. Consider the graph represented Fig 2., $L = \begin{pmatrix} 0 & 0 \\ -1 & 1 \end{pmatrix}$.

Remark 1: When the graph is strongly connected, its Laplacian matrix L is an irreducible singular $Z-$ matrix and $rank(L) = N - 1$ [30].

B. RECURRENT RADIAL BASIS FUNCTION NEURAL NETWORK (RBFNN)

It is important to introduce RBFNN because they are used for universal function approximation and they also exhibits fast learning speed. RBFNN has been used [30], [31] for smooth nonlinear function approximation. Consider the function $G(x) \in R^m$, for m RBFNN nodes, Fig. 3. The RBFNN over a compact set $\nabla \in R$ is expressed as:

$$G(x) = M^T \nabla(x) + \epsilon \quad \forall x \quad \subseteq q \tag{9}$$

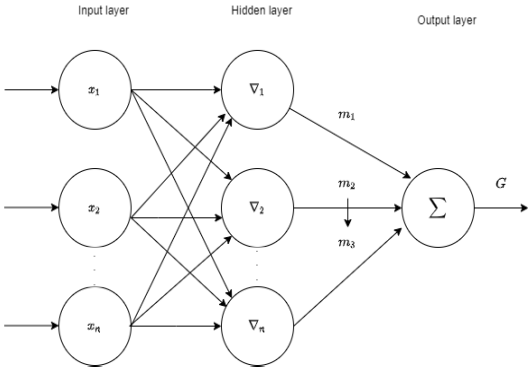

FIGURE 3. RBFNN network architecture.

where x is the RBFNN input, $\nabla(x) = [\nabla_1(x_1), \ldots, \nabla_m(x_m)]^T$ represents the radial basis function vector. The weight vector and approximation error are represented as M^T and ϵ respectively, with $M^T \in R^m$ and $\epsilon \leq \epsilon_*$ where ϵ_* is constant represented by $M = \begin{pmatrix} M_1 & & \\ & \ldots & \\ & & M_m \end{pmatrix}$ and $\epsilon = [\epsilon_1, \ldots, \epsilon_m]^T$

In neural adaptive control, the following results holds [30];

Fact 2:

1) The NN estimation error is bounded by $\|\epsilon\| \leq \epsilon_Z$ on a smooth compact set $\Theta \subset R^N$, where ϵ is a fixed bound [32].
2) Weierstrass higher-order approximation theorem. Select the activation functions $\nabla(x)$ as a complete independent basis. Then the NN estimation error ϵ converges uniformly to zero on Θ as the number of neurons $\eta_i \to \infty, \ i = 1, N$

IV. CONTROL DESIGN

It is desired to maintain inter-agent distance and avoid inter-agent collision. However, the multi-system is underactuated and has strong coupling. Cooperatively carrying a load inline helps to suppress swing in the direction of movement when the load is between the leader and follower [24]. The control block diagram is shown in Fig. 4, which could be scaled to accommodate more than two UAVs.

A. NNGDAC FOR TRAJECTORY TRACKING

To generate the desired acceleration trajectory in the presence of external and load disturbances whereby, inter-agent collision is avoided, it becomes intuitive to adopt a NNGDAC. This concept stems from [29], where a proportional-differential control methodology was used for a single quadrotor uav without load and [33], [34] where multi-UAV is considered without load and obstacle avoidance also. Recall that the translational axis constitute the network which is affected by the load dynamics. Let $\ddot{x}_{ji} = \ddot{\zeta}_{ji}$ be the graph dynamics for any one of the quadrotors. Consequently, in order to generate the virtual inputs, we therefore formulate the global dynamics of both quadrotor system to be governed

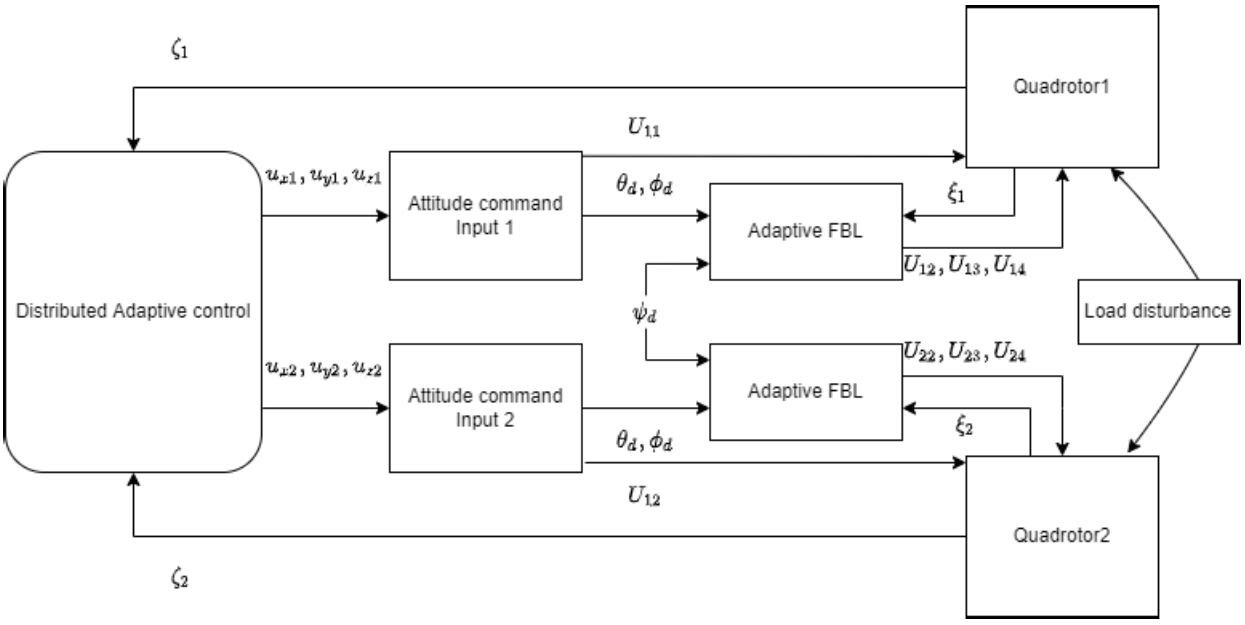

FIGURE 4. Control schematic.

by the Brunovsky form;

$$\begin{aligned} \dot{x}_{1i} &= x_{2i} \\ \dot{x}_{2i} &= \boldsymbol{h}(x) + u_{\zeta_i} + ds \end{aligned} \tag{10}$$

where the state vector is given by $x = [x_{1i}\ x_{2i}]^T$, position vector is given by $x_{1i} = [x_{11}\ x_{12} \ldots x_{1N}]^T \in R^N$, the velocity vector as $x_{2i} = [x_{21}\ x_{22} \ldots x_{2N}]^T \in R^N$, the global dynamics $\boldsymbol{h}(x) = [h_1(x_1)\ h_2(x_2) \ldots h_N(x_N)]^T \in R^N$. $u_{\zeta_i} = [u_1\ u_2 \ldots u_N]^T \in R^N$, $ds_i = [ds_1\ ds_2 \ldots ds_N]^T \in R^N$ input and disturbance respectively.

The external load disturbances is ds and unknown non-linearities is $h(x)$ and $u_{\zeta_i} = (u_x, u_y, u_z)$ represents the this distributive adaptive auxiliary inputs. Whereas the step command or reference generator captured by;

$$\begin{aligned} \dot{x}_{1r} &= x_{2r} \\ \dot{x}_{2r} &= h_r(x_r, t) \end{aligned} \tag{11}$$

where $x_{1r} = [x_{1r}\ \ x_{2r}]^T \in R^2$. It is desirable for both UAVs to maintain the same altitude. Since $R^T = R^{-1}$, from (1), the total thrust for each UAV will be now given by;

$$R(m_q + \frac{m_l}{2})(\ddot{x}_i + g \begin{pmatrix} 0 \\ 0 \\ 1 \end{pmatrix}) = T \begin{pmatrix} 0 \\ 0 \\ 1 \end{pmatrix} \tag{12}$$

It is desired that the control protocol synchronizes the states so as to maintain a safe distance between agents, consider the following assumptions [30]:

Assumption 3: The load disturbance ds_i is bounded for all i. Thus the overall disturbance vector Ds is also bounded by $||Ds|| \leq Ds_Z$ with Ds_Z being a fixed bound.

Assumption 4: Unknown ideal NN weight matrix M is bounded by $||M||_H \leq M_Z$.

Assumption 5: NN activation functions ∇ are bounded by $\forall i$, so that one can write for the overall network that $||\nabla|| \leq \nabla_Z$

Assumption 6: The unknown consensus variable dynamics $||(h_r(x_r, t))|| \leq H_Z, \forall t$ respectively.

Assumption 7: The target trajectory is bounded so that $||x_r(t)|| < X_r(t), ||x_{2r}(t)|| < X_{2r}(t), \forall t$.

Theorem 8: Distributed Adaptive Control Protocol for Synchronization. Consider the networked systems given by (10) under the Assumptions 4.1 - 4.5. The communication digraph being strongly connected. Select the auxiliary control signal so that the local node control protocols are given by [35]:

$$u_{\zeta_i} = kq_i - \hat{h}(x_i) + \frac{\rho_i}{d_i + b_i} e_2 \tag{13}$$

k is the control gain, the adaptive tuning law is taken as;

$$\dot{\hat{M}}_j = -H_i \nabla_i r_i (ds_i + b_i) - \delta H_i \hat{M}_i \tag{14}$$

where the local neighborhood synchronization position and velocity errors for each UAV are given by [36];

$$\begin{aligned} e_{1i} &= \sum_{j \in N_i} a_{ij}(x_{1j} - x_{1i}) + b_i(x_{1r} - x_{1i}) - \eta_{(x,y)}, \\ e_{2i} &= \sum_{j \in N_i} a_{ij}(x_{2j} - x_{2i}) + b_i(x_{2r} - x_{2i}) \end{aligned} \tag{15}$$

respectively, with the pinning gain $b_i \geq 0$, and $b_i > 0$ for at least one i and $\eta_{(x,y)} = norm(\zeta_i)$ specifies inter-agent distance in 2-D. The consensus disagreement error vector is given by;

$$\varphi = \begin{bmatrix} \varphi & \dot{\varphi} \end{bmatrix}^T = \begin{bmatrix} x_{1i} - \underline{1}x_{1r} & x_{2i} - \underline{1}x_{2r} \end{bmatrix}^T$$

where $\underline{1} \in R^N$ is the vector of ones. The global error dynamics may be described as;

$$\begin{aligned} e_1 &= -(\tilde{L})\left(x_{1i} - \underline{1}x_{1r}\right) = -(\tilde{L})\varphi \\ e_2 &= -(\tilde{L})\left(x_{2i} - \underline{1}x_{2r}\right) = -(\tilde{L})\dot{\varphi} \end{aligned} \tag{16}$$

where $\tilde{L} = L + B$, $B = diag(b_i)$ is a diagonal matrix consisting the pinning gains and $e_i \in R^N$ and $e_{2i} \in R^N$, $\forall i$. The following Lemmas applies [30].

Lemma 9: For a strongly connected graph where $B \neq 0$, let

$$\|\varphi\| \leq \frac{\|e_1\|}{\underline{\sigma}(\tilde{L})}, \quad and \quad \|\dot{\varphi}\| \leq \frac{\|e_2\|}{\underline{\sigma}(\tilde{L})}$$

where $\underline{\sigma}(\tilde{L})$ is the minimum singular value of $(\tilde{L})$ and $e = \eta$ if the nodes synchronizes.

Lemma 10: The velocity vector bounded by

$$\|e_2\| \leq \|q\| + \bar{\sigma}(\boldsymbol{\rho})\|e_1\|$$

To minimize the consensus disagreement error and ensure synchronization is reached we will define the sliding mode tracking error given by:

$$q_i = e_{2i} + \rho e_{1i} \tag{17}$$

where, $\rho_i = diag(\rho) > 0$, $\forall i$. Now differentiating (17), yields

$$\dot{q}_i = e_{22i} + \rho_i \dot{e_{1i}} \tag{18}$$

Differentiating (16) yields;

$$\begin{aligned} e_{21} &= -(\tilde{L})\left(x_{2i} - \underline{1}x_{2r}\right) \\ e_{22} &= -(\tilde{L})\left(\dot{x}_{2i} - \underline{1}\dot{h}_r(x_r,t)\right) \end{aligned}$$

Therefore,

$$\begin{aligned} \dot{q}_i = &-(\tilde{L})(h(x) + u_{\zeta_{ij}} + ds_i) \\ &+ (\tilde{L})h_r(x_r,t) + \rho_i e_{2i} \end{aligned} \tag{19}$$

The unknown nonlinearities can be approximated by equation (9). This implies that;

$$h(x) = M^T\nabla(x) + \epsilon \tag{20}$$

we therefore, select the local node's approximation as;

$$\hat{h}(x) = \hat{M}^T\nabla(x) \tag{21}$$

The global error dynamics becomes;

$$\begin{aligned} \dot{q}_i = &-\left(\tilde{L}\right)\left(\hat{h}(x) + u_{\zeta_{ij}}(t) + Ds\right) \\ &+ \left(\tilde{L}\right)\underline{1}h_r(x_r,t) + \boldsymbol{\rho}e_2 \end{aligned} \tag{22}$$

so, considering equation (13), the global control input becomes;

$$\begin{aligned} u_{\zeta_{ij}} &= kq - \hat{M}\nabla(x) + \frac{\boldsymbol{\rho}}{D+B}e_2 \\ \dot{q} &= -\left(\tilde{L}\right)\left(\tilde{h}(x) + kq + Ds\right) \\ &\quad -\left(\tilde{L}\right)\frac{\boldsymbol{\rho}_{ij}}{d_{1j} + b_{ij}}e_2 + \left(\tilde{L}\right)\underline{1}h_r(x_r,t) + \boldsymbol{\rho}e_2 \end{aligned} \tag{23}$$

where $\tilde{h}(x) = h(x) - \hat{h}(x) = \tilde{M}\nabla(x)$ which gives current weight estimate for each individual weight, whereby the weight estimation error gives;

$$\tilde{M} = diag(M_1 - \hat{M}_1, M_2 - \hat{M}_2, \cdots\cdots, M_N - \hat{M}_N)^T$$

recall that $L = D - A$, therefore,

$$\begin{aligned} \dot{q} = &-\left(\tilde{L}\right)\left(\tilde{h}(x) + kq + Ds\right) + \left(\tilde{L}\right) \\ &\times \underline{1}h_r(x_r,t) + A\left(\tilde{D}\right)^{-1}\boldsymbol{\rho}e_2 \end{aligned} \tag{24}$$

where $\tilde{D} = D + B$. Consider the Lyapunov function;

$$V = \frac{1}{2}q^TPq + \frac{1}{2}\tilde{M}^TH^{-1}\tilde{M} + \frac{1}{2}(e_1)^Te_1 \tag{25}$$

where $P = P^T > 0$ and $H^{-1} = H^{-T}$ is a constant matrix therefore the derivative of the Lyapunov function becomes;

$$\dot{V} = q^TP\dot{q} + tr\left\{\tilde{M}^TH^{-1}\dot{\tilde{M}}\right\} + (e_1)^Te_2 \tag{26}$$

Therefore, substituting (20), and (24), in (25)

$$\begin{aligned} \dot{V} = &-q^TP\left(\tilde{L}\right)\left(\tilde{M}^T\nabla(x) + \epsilon + Ds + kq\right) \\ &+ q^TP\left(\tilde{L}\right)\underline{1}h_r(x_r,t) + q^TPA\left(\tilde{D}\right)^{-1}\boldsymbol{\rho}e_2 \\ &+ tr\left\{\tilde{M}^TH^{-1}\dot{\tilde{M}}\right\} + (e_1)^Te_2 \end{aligned} \tag{27}$$

$$\begin{aligned} \dot{V} = &-kq^TP\left(\tilde{L}\right)q - q^TP\left(\tilde{L}\right)\left\{\epsilon + Ds - \underline{1}h_r(x_r,t)\right\} \\ &+ q^TPA\left(\tilde{D}\right)^{-1}\boldsymbol{\rho}e_2 \\ &+ tr\left[\tilde{M}^T\left(H^{-1}\dot{\tilde{M}} - \nabla(x)q^TP\left(\tilde{L}\right)\right)\right] \\ &+ (e_1)^Tq - (e_1)^T\boldsymbol{\rho}e_1 \end{aligned} \tag{28}$$

from (17),

$$\begin{aligned} \dot{V} = &-kq^TP\left(\tilde{L}\right)q - q^TP\left(\tilde{L}\right)\left\{\epsilon + Ds - \underline{1}h_r(x_r,t)\right\} \\ &+ q^TPA\left(\tilde{D}\right)^{-1}\boldsymbol{\rho}(q - \boldsymbol{\rho}e_1) \\ &+ tr\left[\tilde{M}^T\left(H^{-1}\dot{\tilde{M}} - \nabla(x)q^TP\left(\tilde{L}\right)\right)\right] \\ &+ (e_1)^Tq - (e_1)^T\rho e_1 \end{aligned} \tag{29}$$

but $\tilde{L} = \tilde{D} - A$

$$\begin{aligned} \dot{V} = &-kq^TP(\tilde{L})q - q^TP(\tilde{L})\left\{\epsilon + Ds - \underline{1}h_r(x_r,t)\right\} \\ &+ tr\left[\tilde{M}^T\left(H^{-1}\dot{\tilde{M}} - \nabla(x)q^TP\left(\tilde{D}\right)\right)\right] \\ &+ tr\left[\tilde{M}^T\nabla(x)q^TPA\right] + q^TPA\left(\tilde{D}\right)^{-1}\boldsymbol{\rho}q \\ &- q^TPA\left(\tilde{D}\right)^{-1}\boldsymbol{\rho}^2e_1 + (e_1)^Tq - (e_1)^T\boldsymbol{\rho}e_1 \end{aligned} \tag{30}$$

Lemma 11 ([37]): Since $\tilde{L}$ nonsingular Z matrix, the following holds

$$\begin{aligned} q &= \begin{bmatrix} q_1 & q_2 & \cdots & q_N \end{bmatrix}^T = \left(\tilde{L}\right)^{-1}\underline{1} \\ P &= diag\{p_i\} \equiv diag\{1/q_i\} \end{aligned}$$

Then $P > 0$ and the symmetric positive definite matrix Q is given by;

$$Q = P(\tilde{L}) + (\tilde{L})^T P \tag{31}$$

recall that L is irreducible and $b_i > 0$, so from Lemma 4.3,

$$\begin{aligned}\dot{V} = &-\frac{1}{2}kq^T Qq - q^T P\left(\tilde{L}\right)\left\{\epsilon + Ds - \underline{1}h_r(x_r,t)\right\}\\ &+tr\left[\tilde{M}^T\left(H^{-1}\dot{\tilde{M}} - \nabla(x)\,q^T P\left(\tilde{D}\right)\right)\right]\\ &+tr\left[\tilde{M}^T\nabla(x)\,q^T PA\right] + q^T PA\left(\tilde{D}\right)^{-1}\boldsymbol{\rho}q\\ &-q^T PA\left(\tilde{D}\right)^{-1}\boldsymbol{\rho}^2 e_1 + (e_1)^T q - (e_1)^T\boldsymbol{\rho}e_1\end{aligned} \tag{32}$$

where $Q = Q^T > 0$. Now applying (14) and taking the norm of both sides yields

$$\begin{aligned}\dot{V} \le &-\frac{1}{2}k\underline{\sigma}(Q)\|q\|^2 + \bar{\sigma}(P)\bar{\sigma}\left(\tilde{L}\right)H_Z\|q\|\\ &+\delta M_Z\left\|\tilde{M}\right\|_H - \delta\left\|\tilde{M}\right\|_H^2\\ &+\phi_Z\bar{\sigma}(P)\bar{\sigma}(A)\left\|\tilde{M}\right\|_H\|q\|\\ &+\frac{\bar{\sigma}(P)\bar{\sigma}(A)\bar{\sigma}(\boldsymbol{\rho})}{\underline{\sigma}\left(\tilde{D}\right)}\|q\|^2\\ &+\left(1+\frac{\bar{\sigma}(P)\bar{\sigma}(A)\bar{\sigma}\left(\boldsymbol{\rho}^2\right)}{\underline{\sigma}\left(\tilde{D}\right)}\right)\|q\|\|e_1\| - \underline{\sigma}(\boldsymbol{\rho})\|e_1\|^2\end{aligned} \tag{33}$$

where $T_Z = Ds_Z + \epsilon_Z + H_Z$, already defined in Fact 3.1 and Assumptions 4.1 - 4.5. Maximum and minimum singular values of a matrix Z is denoted by $\bar{\sigma}(Z)$ and $\underline{\sigma}(Z)$ respectively and $\|Z\|_N = \sqrt{tr\{Z^T Z\}}$ with $tr\{\cdot\}$. (34), as shown at the bottom of the next page, which can be re-written as;

$$\dot{V} \le -s^T Cs + c^T s \tag{35}$$

As we can see $\dot{V} \le 0$ iff $C \ge 0$, so

$$\|s\| > \frac{\|c\|}{\underline{\sigma}(C)} \tag{36}$$

Based on the Lyapunov equation, for $\dot{V} \le 0$, therefore (34) becomes

$$\begin{aligned}\dot{V} \le &-\underbrace{\begin{bmatrix}\|e_1\| & \|q\| & \left\|\tilde{M}\right\|_H\end{bmatrix}\begin{bmatrix}\rho & 1 & 0\\ 1 & \rho & \gamma\\ 0 & \gamma & \delta\end{bmatrix}}_{C}\begin{bmatrix}\|e_1\|\\ \|q\|\\ \left\|\tilde{M}\right\|_H\end{bmatrix}\\ &+\begin{bmatrix}0 & \bar{\sigma}(P)\bar{\sigma}\left(\tilde{L}\right)T_Z & \delta W_M\end{bmatrix}\begin{bmatrix}\|e_1\|\\ \|q\|\\ \left\|\tilde{M}\right\|_H\end{bmatrix}\end{aligned}$$

Since singular values are equivalent to eigen values, for symmetric positive definite matrix, $C \ge 0$ we select, $\boldsymbol{\rho} = \rho I$, $\rho = \sqrt{\frac{\alpha\left(\tilde{D}\right)}{\bar{\sigma}(P)\bar{\sigma}(A)}}$, $k = \frac{2}{\alpha(Q)}\left(\frac{1}{\rho} + \rho\right) > 0$, and $\gamma = \frac{1}{2}\nabla_m\bar{\sigma}(P)\bar{\sigma}(A)$.

According to Geršhgorin circle's theorem; $\underline{\sigma}(C) \ge \delta - \gamma$ with $0 < \gamma \le \delta \le \rho - 1$. Hence, $s(t)$ is UUB. Consequently, $\|s\|_1 \ge \|s\|_2 \ge \cdots \ge \|s\|_\infty$ with sufficient conditions;

$$\|q\| > \frac{T_Z\bar{\sigma}(P)\bar{\sigma}\left(\tilde{L}\right) + \delta M_Z}{\delta - \frac{1}{2}\nabla_m\bar{\sigma}(P)\bar{\sigma}(A)} \tag{37}$$

or

$$\|e_1\| > \frac{T_Z\bar{\sigma}(P)\bar{\sigma}\left(\tilde{L}\right) + \delta M_Z}{\delta - \frac{1}{2}\nabla_m\bar{\sigma}(P)\bar{\sigma}(A)} \tag{38}$$

or

$$\left\|\tilde{M}\right\| > \frac{T_Z\bar{\sigma}(P)\bar{\sigma}\left(\tilde{L}\right) + \delta M_Z}{\delta - \frac{1}{2}\nabla_m\bar{\sigma}(P)\bar{\sigma}(A)} \tag{39}$$

which also shows UUB of $q(t)$, $e_1(t)$, $\tilde{M}(t)$. Therefore, from Lemma 4.1, the boundedness of q and e_1 implies bounded e_2. Now Lemma 4.1 shows that the consensus error vector $\varphi(t)$ is UUB. Hence $x_r(t)$ is cooperative UUB.

B. ATTITUDE CONTROL DESIGN

The load disturbances causes changes in the dynamics which can be mitigated by adaptive control methods, according to [15]. Considering the references therein, an AFBL is utilized to control of each UAV attitude subsystem ξ_i. For the attitude subsystem;

$$\ddot{\xi}_i = f(\xi) + gu \tag{40}$$

let, $u = g^{-1}(-f(\xi) + \rho + \chi)$ substituting in (40) gives

$$\dot{\xi}_i = \rho_s + \chi \tag{41}$$

where χ is the lumped uncertainties induced. The error dynamics is given by;

$$e_\xi = \dot{\xi}_d - \dot{\xi} \tag{42}$$

let

$$\tilde{\chi} = \hat{\chi} - \chi \tag{43}$$

be the error between the lumped uncertainty and its estimated value, an appropriate Lyapunov function can be defined as:

$$V = \frac{1}{2}e_\xi^2 + \frac{1}{2}\nu\tilde{\chi}^2 \tag{44}$$

where ν is the adaptation gain. Therefore;

$$\dot{V} = e_\xi\dot{e_\xi} + \nu\tilde{\chi}\dot{\tilde{\chi}}$$

let $\rho_s = \ddot{\xi} - \hat{\chi} + ke_\xi$ Therefore,

$$\dot{V} = -ke_\xi^2 - \tilde{\chi}(e_\xi + \nu\dot{\tilde{\chi}})$$

for $\dot{V} \le 0$, $k > 0$ and the adaptation gain is thus,

$$\dot{\hat{\gamma}} = -\nu^{-1}e_\xi \tag{45}$$

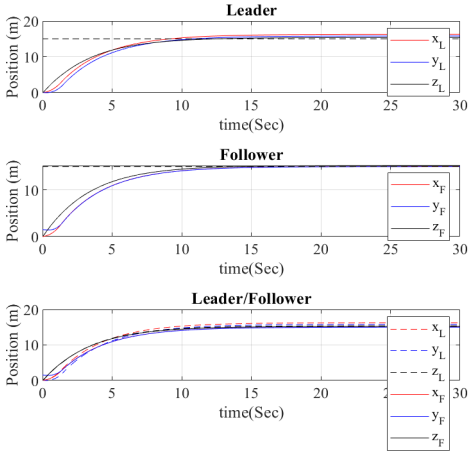

FIGURE 5. Trajectory of leader-follower.

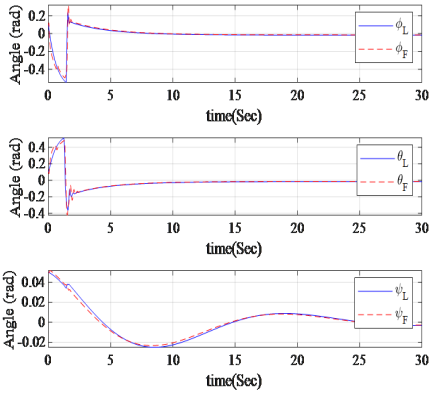

FIGURE 6. Leader-follower orientation angles.

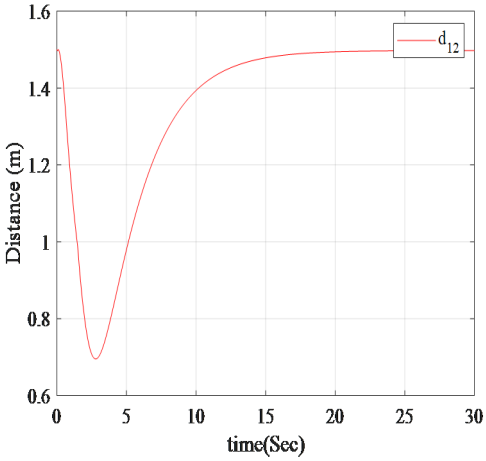

FIGURE 7. Inter-agent distance.

V. OBSTACLE AVOIDANCE

Obstacle avoidance is a key feature for UAVs moving in a cluttered environment. However, conventional potential field methods used for obstacle avoidance developed for ground robots, are not suitable for aerial vehicles due to their fast movement and inherent instability [38]. We therefore utilize a modified repulsive potential with virtual force E whenever there is an obstacle in the path of the MUAVS, defined as [39];

$$O_a = \sum_{i=1}^{2} E_i \tag{46}$$

where

$$E = \begin{cases} E_{rep}(\zeta) + E_{vir}(\zeta) & \rho \leq \rho_{obs} \\ 0 & \rho > \rho_{obs} \end{cases}$$

where

$$E_{rep}(\zeta) = -K_e(1 - \frac{\rho}{\rho_{obs}})(\frac{\zeta_{obs} - \zeta}{\rho^3})$$

$$E_{vir}(\zeta) = -K_{vir}\frac{1}{\rho}$$

where $-K_e$ and $-K_{vir}$ are constants. ρ_{obs} is the quadrotor minimal distance which has a repulsive effect must be greater than the inter-agent distance, i.e ($\rho_{obs} > \eta_{(x,y)}$) to avoid

$$\begin{aligned}
\dot{V} \leq & -\left[\|e_1\| \ \|q\| \ \left\|\tilde{M}\right\|_H \right] \\
& \times \begin{bmatrix} \underline{\sigma}(\boldsymbol{\rho}) & \frac{1}{2}\left(1 + \frac{\bar{\sigma}(P)\bar{\sigma}(A)\bar{\sigma}(\boldsymbol{\rho}^2)}{\underline{\sigma}\left(\tilde{D}\right)}\right) \\ \frac{1}{2}\left(1 + \frac{\bar{\sigma}(P)\bar{\sigma}(A)\bar{\sigma}(\boldsymbol{\rho}^2)}{\underline{\sigma}\left(\tilde{D}\right)}\right) & \left(\frac{1}{2}k\underline{\sigma}(Q) - \frac{\bar{\sigma}(P)\bar{\sigma}(A)\bar{\sigma}(\boldsymbol{\rho})}{\underline{\sigma}\left(\tilde{D}\right)}\right) \cdots \\ 0 & \frac{1}{2}\phi_L\bar{\sigma}(P)\bar{\sigma}(A) \end{bmatrix} \\
& \begin{bmatrix} 0 \\ \cdots \ \frac{1}{2}\phi_L\bar{\sigma}(P)\bar{\sigma}(A) \\ \delta \end{bmatrix} \begin{bmatrix} \|e_1\| \\ \|q\| \\ \left\|\tilde{M}\right\|_H \end{bmatrix} \\
& + \left[0 \ \bar{\sigma}(P)\bar{\sigma}\left(\tilde{L}\right) T_Z \ \delta M_Z \right] \begin{bmatrix} \|e_1\| \\ \|q\| \\ \left\|\tilde{M}\right\|_H \end{bmatrix}
\end{aligned} \tag{34}$$

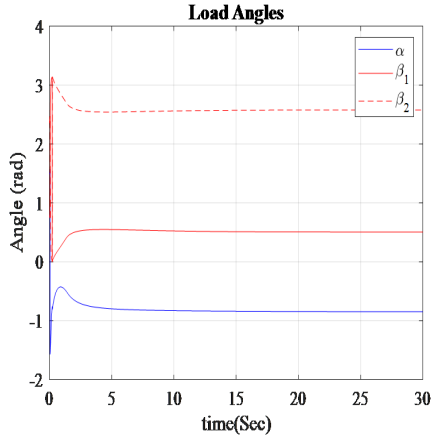

FIGURE 8. Load orientation angles.

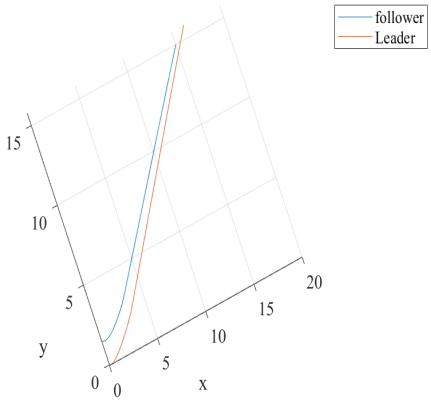

FIGURE 9. 3-D plot.

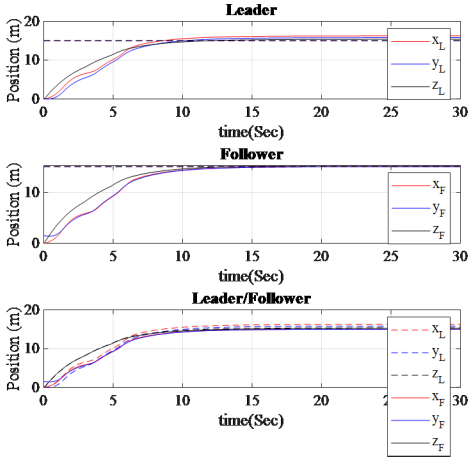

FIGURE 10. Trajectory of leader-follower.

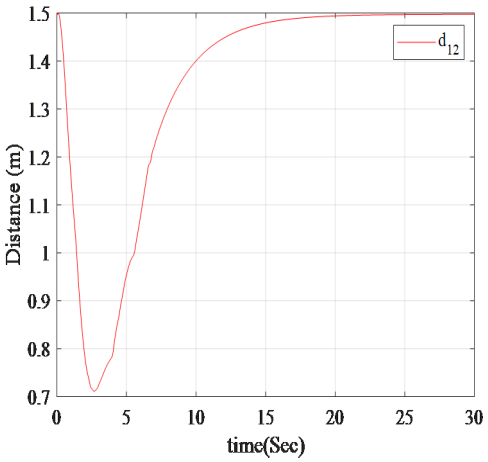

FIGURE 11. Inter-agent distance.

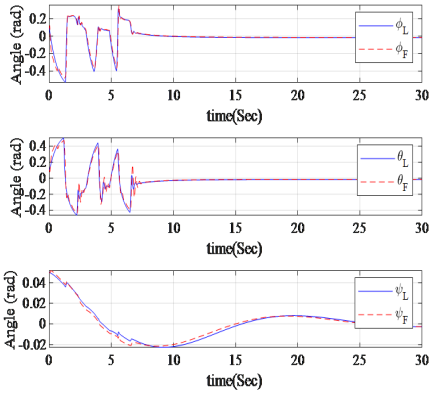

FIGURE 12. Leader-follower orientation angles.

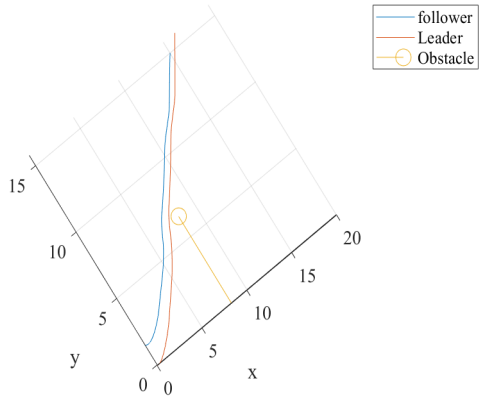

FIGURE 13. 3-D plot.

conflict. The distance between the quadrotor and the obstacle is given by;

$$\rho = \sqrt{(\zeta - \zeta_{obs})^2}$$

VI. SIMULATION RESULTS

We utilized UAV parameter values for Parrot AR.Drone [14]. To demonstrate the effectiveness of the control algorithm, we present simulation results for the system firstly without obstacle avoidance. Both UAVs are kept apart with a initial positions $\zeta = [0, 0, 0]$ and $\zeta = [1, 0, 0]$ for the leader and follower respectively while final was position specified as $\zeta = [15, 15, 15]$. Fig. 5 shows position of the MUAVL during trajectory tracking without activating obstacle avoidance. Evidently, our proposed strategy can effectively maintain as

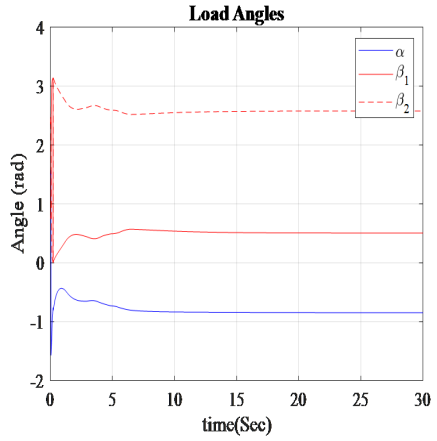

FIGURE 14. Load orientation angles.

safe distance between agent while containing the disturbance and hence load swing. Attitude tracking is also achieved, Fig. 6.

Obviously, there is a negligible orientation tracking error which could be improved upon in future. Fig. 7 shows that inter-agent distance between the leader and follower is maintained. The load angles are shown in Fig. 8, with $\beta_1 = 30°$, and $\beta_2 = 33.6°$ of the follower to the horizontal. The discrepancy emanating from the a slight difference in height which is also negligibly small and does not compromise the aim of this work. However, with $\alpha = 48.6°$ to the vertical, due to the fact that the follower is not directly behind the leader UAV. A 3-D plot is shown for visual purpose, Fig. 9.

To demonstrate obstacle avoidance, an obstacle is placed at a point centered at $\zeta_{obs} = [8.2, 7.4, 9]$ in the path of the MUAVLs. Fig. 10 shows the position trajectory tracking when the obstacle avoidance is activated. Note that the leader deviates slightly while the follower also deviates sufficiently enough such that the inter-agent distance is not compromised. Evident in Fig. 11, the inter-agent distance between the leader and follower are maintained. Attitude orientation angles of the leader and follower are shown in Fig. 12 with a 3-D plot of the position in. Fig. 13 for visual purpose. As can be seen in Fig. 14, the load angles are maintained after a slight disturbance due to obstacle avoidance.

VII. CONCLUSION

A Neural Network Graph-theoretic Distributed Adaptive Control (NNGDAC) algorithm which is equipped with a modified virtual force artificial potential field for obstacle avoidance is used for tracking a Multi-agent UAV Load system (MUAVLs) in the presence of load disturbances. A local Adaptive Feedback Linearization (AFBL) controller is also designed for the rotational axis which is verified by simulation results. However, tilt-wing/rotor UAVs are generally fully actuated, therefore, there is need to investigate how additional input could be utilized to cater for inherent problems associated with MUAVLs to reduce control complexity. Our future work includes investigating actuator fault in the development of a fault tolerant controller.

REFERENCES

[1] A. Aliyu, M. Elshafei, A.-W.-A. Saif, and M. Dhaifullah, "Performance evaluation of quadrotor with tilted rotors under wind gusts," in *Proc. IEEE Int. Conf. Adv. Intell. Mechatronics (AIM)*, Jul. 2016, pp. 294–299.
[2] T. Lee, "Geometric control of quadrotor UAVs transporting a cable-suspended rigid body," *IEEE Trans. Control Syst. Technol.*, vol. 26, no. 1, pp. 255–264, Jan. 2018.
[3] J. Gimenez, D. C. Gandolfo, L. R. Salinas, C. Rosales, and R. Carelli, "Multi-objective control for cooperative payload transport with rotorcraft UAVs," *ISA Trans.*, vol. 80, pp. 491–502, Sep. 2018.
[4] L. R. Salinas, J. Gimenez, C. Rosales, and D. C. Gandolfo, "Null-space-based path-following control for cooperative payload transport using multiple rotorcraft UAVs," in *Proc. Int. Conf. Unmanned Aircr. Syst. (ICUAS)*, 2018, pp. 631–638.
[5] J. Geng and J. W. Langelaan, "Implementation and demonstration of coordinated transport of a slung load by a team of rotorcraft," in *Proc. AIAA Scitech Forum*, San Diego, CA, USA, Jan. 2019.
[6] Y. H. Tan, S. Lai, K. Wang, and B. M. Chen, "Cooperative control of multiple unmanned aerial systems for heavy duty carrying," *Annu. Rev. Control*, vol. 46, pp. 44–57, Jan. 2018.
[7] N. S. Zuniga, F. Munoz, M. A. Marquez, E. S. Espinoza, and L. R. G. Carrillo, "Load transportation using single and multiple quadrotor aerial vehicles with swing load attenuation," in *Proc. Int. Conf. Unmanned Aircr. Syst. (ICUAS)*, Jun. 2018, pp. 269–278.
[8] Y. N. I. Alothman, "Optimal control of multiple quadrotors for transporting a cable suspended payload by," Ph.D. dissertation, Univ. Essex, Colchester, U.K., 2018.
[9] M. Gassner, T. Cieslewski, and D. Scaramuzza, "Dynamic collaboration without communication: Vision-based cable-suspended load transport with two quadrotors," in *Proc. IEEE Int. Conf. Robot. Autom. (ICRA)*, May 2017, pp. 5196–5202.
[10] B. Shirani, M. Najafi, and I. Izadi, "Cooperative load transportation using multiple UAVs," *Aerosp. Sci. Technol.*, vol. 84, pp. 158–169, Jan. 2019.
[11] A. S. Aghdam, M. B. Menhaj, F. Barazandeh, and F. Abdollahi, "Cooperative load transport with movable load center of mass using multiple quadrotor UAVs," in *Proc. 4th Int. Conf. Control, Instrum., Autom. (ICCIA)*, Jan. 2016, pp. 23–27.
[12] I. H. B. Pizetta, A. S. Brandao, and M. Sarcinelli-Filho, "Cooperative quadrotors carrying a suspended load," in *Proc. Int. Conf. Unmanned Aircr. Syst. (ICUAS)*, Jun. 2016, pp. 1049–1055.
[13] K. Mohammadi, M. Jafarinasab, S. Sirouspour, and E. Dyer, "Decentralized motion control in a cabled-based multi-drone load transport system," in *Proc. IEEE/RSJ Int. Conf. Intell. Robots Syst. (IROS)*, Oct. 2019, pp. 4198–4203.
[14] I. H. B. Pizetta, A. S. Brand ao, and M. Sarcinelli-Filho, "Avoiding obstacles in cooperative load transportation," *ISA Trans.*, vol. 91, pp. 253–261, Aug. 2019.
[15] I. Palunko, P. Cruz, and R. Fierro, "Agile load transportation: Safe and efficient load manipulation with aerial robots," *IEEE Robot. Autom. Mag.*, vol. 19, no. 3, pp. 69–79, Sep. 2012.
[16] C. Meissen, K. Klausen, M. Arcak, T. I. Fossen, and A. Packard, "Passivity-based formation control for UAVs with a suspended load," *IFAC-PapersOnLine*, vol. 50, no. 1, pp. 13150–13155, 2017.
[17] K. Klausen, C. Meissen, T. I. Fossen, M. Arcak, and T. A. Johansen, "Cooperative control for multirotors transporting an unknown suspended load under environmental disturbances," *IEEE Trans. Control Syst. Technol.*, vol. 28, no. 2, pp. 653–660, Mar. 2018.
[18] R. Hahnemann, D. Schindler, M. Kamel, R. Siegwart, and J. Nieto, "A decentralized multi-agent unmanned aerial system to search, pick up, and relocate objects," in *Proc. 15th IEEE Int. Symp. Saf., Secur. Rescue Robot., Conf. (SSRR)*, Oct. 2017, pp. 123–128.
[19] K. K. Dhiman, A. Abhishek, and M. Kothari, "Cooperative load control and transportation," in *Proc. AIAA Inf. Systems-AIAA Infotech Aerosp.*, Jan. 2018, p. 895.
[20] H. I. Lee, D. W. Yoo, B. Y. Lee, G. H. Moon, D. Y. Lee, M. J. Tahk, and H. S. Shin, "Parameter-robust linear quadratic Gaussian technique for multi-agent slung load transportation," *Aerosp. Sci. Technol.*, vol. 71, pp. 119–127, Dec. 2017.
[21] J. C. Erskine, "Wrench analysis of cable-suspended parallel robots actuated by quadrotors UAVs," *J. Mech. Robot., Amer. Soc. Mech. Eng.*, vol. 11, no. 2, pp. 020909-1–020909-12, 2019.
[22] G. Wu and K. Sreenath, "Geometric control of multiple quadrotors transporting a rigid-body load," in *Proc. 53rd IEEE Conf. Decis. Control*, Dec. 2014, pp. 6141–6148.

[23] L. Qian and H. H. Liu, "Path following control of multiple quadrotors carrying a rigid-body slung payload," in *Proc. AIAA Scitech Forum*, San Diego, CA, USA, Jan. 2019.
[24] D. K. Villa, A. S. Brandao, and M. Sarcinelli-Filho, "A survey on load transportation using multirotor UAVs," *J. Intell. Robotic Syst.*, vol. 98, no. 2, pp. 1–30, 2019.
[25] G. Wen, C. L. P. Chen, and Y.-J. Liu, "Formation control with obstacle avoidance for a class of stochastic multiagent systems," *IEEE Trans. Ind. Electron.*, vol. 65, no. 7, pp. 5847–5855, Jul. 2017.
[26] R. Olfati-Saber, "Flocking for multi-agent dynamic systems: Algorithms and theory," *IEEE Trans. Autom. Control*, vol. 51, no. 3, pp. 401–420, Mar. 2006.
[27] O. Saif, I. Fantoni, and A. Zavala-Rio, "Real-time flocking of multiple-quadrotor system of systems," in *Proc. 10th Syst. Syst. Eng. Conf. (SoSE)*, May 2015, pp. 286–291.
[28] H. Voos, "Nonlinear control of a quadrotor micro-UAV using feedback-linearization," in *Proc. IEEE Int. Conf. Mechatronics*, Apr. 2009, pp. 1–6.
[29] Z. Zuo, "Trajectory tracking control design with command-filtered compensation for a quadrotor," *IET Control Theory Appl.*, vol. 4, no. 11, pp. 2343–2355, Nov. 2010.
[30] F. L. Lewis, H. Zhang, K. Hengster-Movric, and A. Das, *Cooperative Control of Multi-Agent Systems: Optimal and Adaptive Design Approaches*. London, U.K.: Springer-Verlag, 2014.
[31] H. Shi, M. Wang, and C. Wang, "Leader-follower formation learning control of discrete-time nonlinear multiagent systems," *IEEE Trans. Cybern.*, early access, Oct. 4, 2021, doi: 10.1109/TCYB.2021.3110645.
[32] K. Hornik, M. Stinchcombe, and H. White, "Multilayer feedforward networks are universal approximators," *Neural Netw.*, vol. 2, no. 5, pp. 359–366, 1989.
[33] J. Ghommam, L. F. Luque-Vega, M. Saad, and B. Castillo-Toledo, "Three-dimensional distributed tracking control for multiple quadrotor helicopters," *J. Franklin Inst.*, vol. 353, no. 10, pp. 2344–2372, 2016.
[34] J. Wang, X. Ma, H. Li, and B. Tian, "Self-triggered sliding mode control for distributed formation of multiple quadrotors," *J. Franklin Inst.*, vol. 357, no. 17, pp. 12223–12240, Nov. 2020.
[35] A. Das and F. L. Lewis, "Cooperative adaptive control for synchronization of second-order systems with unknown nonlinearities," *Int. J. Robust Nonlinear Control*, vol. 21, no. 13, pp. 1509–1524, 2011.
[36] S. Khoo, L. Xie, and Z. Man, "Robust finite-time consensus tracking algorithm for multirobot systems," *IEEE/ASME Trans. Mechatronics*, vol. 14, no. 2, pp. 219–228, Apr. 2009.
[37] Z. Qu, *Cooperative Control of Dynamical Systems: Applications to Autonomous Vehicles*. London, U.K.: Springer-Verlag, 2009.
[38] A. C. Woods and H. M. La, "A novel potential field controller for use on aerial robots," *IEEE Trans. Syst., Man, Cybern., Syst.*, vol. 49, no. 4, pp. 665–676, Apr. 2019.
[39] A. Ma'Arif, W. Rahmaniar, M. A. M. Vera, A. A. Nuryono, R. Majdoubi, and A. Cakan, "Artificial potential field algorithm for obstacle avoidance in UAV quadrotor for dynamic environment," in *Proc. IEEE Int. Conf. Commun., Netw. Satell. (COMNETSAT)*, Jul. 2021, pp. 184–189.

ABDULRAHMAN ALIYU received the B.Eng. degree in electrical engineering from Bayero University Kano, Nigeria, and the M.Sc. degree in systems and control engineering from the King Fahd University of Petroleum and Minerals, Dhahran, Saudi Arabia, in 2016, where he is currently pursuing the Ph.D. degree in systems and control engineering. His research interests include artificial intelligence for robotics, nonlinear control, multiagent, and complex systems.

SAMI EL FERIK received the B.Sc. degree in electrical engineering from Laval University, Quebec, Canada, and the M.S. and Ph.D. degrees from the Control and Automation Electrical and Computer Engineering Department, Ecole Polytechnique, University of Montreal, Montreal, Canada.

He is currently a Professor with the Control and Instrumentation, Engineering Department and the Director of the Interdisciplinary Research Center for Smart Mobility and Logistics, KFUPM. His Ph.D. work was on flexible manufacturing systems modeling and control and was co-supervised with mechanical engineering. His master's degree on identification and optimal control of a stochastic electrical load. After completion of his Ph.D. degree and a postdoctoral researcher positions in analysis and control of discrete event systems, he worked at Pratt and Whitney Canada as a Senior Staff Control Analyst with the Research and Development Center of Systems, Controls, and Accessories. His research interests include sensing, monitoring, and control with strong multidisciplinary research and applications. His research contributions are in control of autonomous multi-agent systems, biological models of fleet of unmanned aerial vehicles, process control and control loop performance-monitoring, control of systems with delays, modeling and control of stochastic systems, analysis of network stability, condition monitoring, and condition-based maintenance.